

## Laser Light Scattering: Some Recent Developments

Standard Article

Wu Chi<sup>1</sup> and Gong Xiangjun<sup>1</sup>

<sup>1</sup>The Chinese University of Hong Kong, Shatin, New Territories, Hong Kong, People's Republic of China

Copyright © 2010 by John Wiley & Sons, Inc. All rights reserved.

[DOI](#): 10.1002/0471440264.pst407

Article Online Posting Date: January 29, 2010

[Abstract](#) | Full Text: [HTML](#)

### Abstract

This review summarizes some recent developments in the characterization of some special intractable macromolecules in solution by a combination of static and dynamic laser light scattering (LLS). Since both static and dynamic LLS are theoretically well established, we have limited this review on experimental details, such as the design of a high temperature LLS spectrometer, the clarification of polymer solutions, complementary apparatuses such as a novel differential refractometer, and portable particle sizer.

[\[Top of Page\]](#)

### 1. Introduction

In a broad definition, laser light scattering (LLS) could be grouped as inelastic (eg, Raman, fluorescence, and phosphorescence) and elastic (no absorption) light scattering. However, in polymer and colloid science, LLS is normally referred to in terms of static (elastic) or dynamic (quasi-elastic) measurements, or both (1). Static LLS as a classic and absolute analytical method measures the time-average intensity and it has been long and widely used to characterize both synthetic and natural macromolecules (2, 3). On the other hand, dynamic LLS measures the intensity fluctuation. This is where the word *dynamic* comes from. The visibility of the scattering objects (macromolecules or colloidal particles) in LLS depends on the refractive index difference ( $d_n$ ) between the scattering object and dispersion medium.

In the past two decades, thanks to the advancement stable laser, ultrafast electronics and personal computer, LLS, especially dynamic LLS, has evolved from a very special instrument for physicists and physical chemists to a routine analytical tool in polymer laboratories or even to a daily quality-control device in production lines. Commercially available research-grade LLS instruments (eg, ALV, Germany and Brookhaven, NY) nowadays are capable of making static and dynamic measurements simultaneously for studies of colloidal particles in suspensions or macromolecules in solutions as well as in gels and viscous media.

Considering the interaction of laser light (an electromagnetic radiation) with matter, we can describe it in terms of two fundamental quantities: the momentum transfer ( $\hbar\mathbf{K}$ ) and the energy transfer ( $\hbar\Delta\omega$ ), obeying the conservation equation:

$$\hbar\mathbf{K} = \hbar(k_I - k_S) \text{ and } \hbar\Delta\omega = \hbar(\omega_I - \omega_S) \quad (1)$$

where  $\hbar = h/2\pi$  with  $h$  being Planck's constant;  $k_I, k_S$ , and  $\omega_I, \omega_S$  are, respectively, the incident and scattered wave vectors with magnitudes  $2\pi/\lambda_I, 2\pi/\lambda_S$  and angular frequencies  $2\pi\nu_I, 2\pi\nu_S$ . For structural and dynamic information, we can use  $R \sim K^{-1}$  as a spatial resolution ruler in static LLS to probe the sizes of colloidal particles and macromolecules; and  $\tau \sim 1/\Delta\nu = 1/(\nu_I - \nu_S)$  as a characteristic time range in dynamic LLS to measure the relaxation of colloids in suspension or macromolecules in solution.

The amplitude of scattering vector  $\mathbf{K}$ , written as  $q (= 4\pi \sin(\theta/2)/\lambda)$ , is a pertinent parameter. In principle, one can change either the scattering angle  $\theta$  or the wavelength  $\lambda$  of the beam in the scattering medium to alter  $q$ . However, in LLS, it is not practical to vary  $\mathbf{K}$  by  $\lambda$ . Therefore,  $q$  is typically varied by  $\theta$  in the range  $15^\circ - 160^\circ$ , implying that in static LLS we can only measure the size ( $R$ ) down to about tens of nanometers, much larger than that in small angle x-ray scattering (4). In dynamic LLS, translational motions of macromolecules or particles within the size range 1–1000 nm can be measured. The characteristic time of relaxation in dynamic LLS, which include translational, rotational, and internal motions, could vary from seconds to tens of nanoseconds (5). There are different ways to measure the characteristic time (6), but we shall discuss only the commonly used self-beating intensity-intensity time correlation spectroscopy.

Many reviews, books, proceedings, and chapters have been published on the topic. The present article can be viewed as a long abstract of that text. Serious LLS users should consult (1-3) and other books, rather than proceedings or articles, as reference materials. In particular, the first monograph on the theoretical aspects of dynamic laser light scattering by Berne and Pecora (7) is highly recommended because it remains as the best source reference. Here, we will concentrate only on the experimental detail. Often, static and dynamic LLS are used separately: namely, polymer chemists are more familiar with static LLS and only use dynamic LLS to size particles, whereas polymer physicists are not accustomed to precise static LLS measurements and sample preparation. This seriously limits their application. This article specially deals with this problem by using several typical examples to show how static and dynamic LLS can be combined to extract more information, such as the characterization of molar mass distribution, estimation of composition distribution of a copolymer, the adsorption/grafting of polymer chains on colloidal particle surface, and the self-assembled nanostructure of block copolymers.

[\[Top of Page\]](#)

## 2. Static Laser Light Scattering

For the convenience of discussion, both macromolecules and colloidal particles are referred as *particles* hereafter. When a light beam  $I_{\text{INC}}$  hit a solution, the excess Rayleigh ratio,  $R_{\text{VV}}(q)$ , of the solute particles for the vertically polarized incident and scattering lights has the form

$$\frac{HC}{R_{\text{VV}}(q)} \approx \frac{1}{M_w P(q)} \quad (2)$$

where  $H [= 4\pi^2 n_0^2 (\partial n/\partial C)_{\text{TP}}^2 / (N_A \lambda_0^4)]$  is an optical constant for a given polymer solution and a laser light source,  $M_w (= \int_0^\infty f_w(M)M dM / \int_0^\infty f_w(M) dM)$  is the weight

average molar mass and  $f_w(M)$  is the weight distribution of molar mass. The scattering factor  $P(q)$  for particles with different shapes have been previously derived (8, 9) and graphically displayed (10). It is related to  $q$  and the root-mean square  $z$ -average radius of gyration  $\langle R_g^2 \rangle_z^{1/2}$ , or write as  $\langle R_g \rangle$ , where  $\langle R_g^2 \rangle_z$  is defined as  $\int_0^\infty f_w(M)MR_g^2 dM / \int_0^\infty f_w(M)M dM$ . When  $\langle R_g \rangle$  is smaller than  $1/q$ , i.e.  $q\langle R_g \rangle \ll 1$ , we have

$$P(q) \approx 1 - \frac{1}{3}q^2 R_g^2 + \dots \quad (3)$$

It can be shown that equation 3 is not only valid for the Gaussian chain but also for particles with an arbitrary shape as long as  $q\langle R_g \rangle \ll 1$ . Considering the interparticle interference between the scattered lights, Debye (11) showed in 1947 that the concentration dependence can be virial expanded as a power series in the concentration, whose combination with equations 2 and 3 leads to

$$\frac{HC}{R_{VV}(q)} = \frac{1}{M_w} \left( 1 + \frac{1}{3} \langle R_g^2 \rangle_z q^2 + \dots \right) + 2A_2 C + \dots \quad (4)$$

where  $A_2$  is the second virial coefficient. This is the most basic equation in static LLS. With  $R_{VV}(q)$  measured over a series of  $C$  and  $q$ , one can obtain  $\langle R_g \rangle$  and  $A_2$ , respectively, from the slopes of  $[HC/R_{VV}(q)]_{C \rightarrow 0}$  versus  $q^2$  and  $[HC/R_{VV}(q)]_{q \rightarrow 0}$  versus  $C$ ; and  $M_w$  from  $[HC/R_{VV}(q)]_{C \rightarrow 0, q \rightarrow 0}$ . The Zimm plot,  $HC/R_{VV}(q)$  versus  $(q^2 + kC)$  with  $k$  an adjustable constant, allows the extrapolations of  $q \rightarrow 0$  and  $C \rightarrow 0$  to be made on a single grid (12). Figure 1 shows a typical Zimm plot for thermally sensitive and biocompatible poly(*N*-vinylcaprolactam) in water at 25 °C (13).

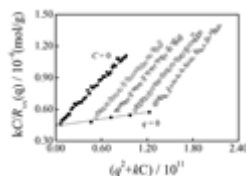


**Figure 1.** Typical Zimm plot for thermally sensitive and biocompatible poly(*N*-vinyl-caprolactam) ( $M_w = 2.34 \times 10^6$  g/mol,  $\langle R_g \rangle = 79$  nm and  $A_2 = 1.59 \times 10^{-4}$  mol mL/g<sup>2</sup>) in water at 25 °C.

It should be noted that equation 4 is valid under the restriction that the solution exhibits no absorption, no fluorescence, and no depolarized scattering. As for anisotropic rigid or rigid-like rods with a depolarized scattering, readers should refer to the excellent review article of Russo and the references therein (14). As for the correction of absorption and fluorescence, readers are advised to refer to the characterization of Kevel in concentrated sulfuric acid by Ying and co-workers (15-17). In practice, the Rayleigh ratio is determined by a relative method, namely, by measuring the scattering intensity of a standard, for example, benzene or toluene, we can calculate the Rayleigh ratio of a solution by

$$R_{VV}(q) = R_{VV}^o(q) \frac{\langle I \rangle_{\text{solution}} - \langle I \rangle_{\text{solvent}}}{\langle I^o \rangle} \left( \frac{n}{n^o} \right)^\nu \quad (5)$$

where the superscript "o" denotes the standard and  $\langle I \rangle$  is the time-averaged scattering intensity. The term  $(n/n^o)^\nu$  is a refraction correction for the scattering volume and  $1 \leq \nu \leq 2$ , depending on the detection optics. If a slit is used, we only need to correct the refraction in one direction ( $\nu = 1$ ). On the other hand, if a pinhole with a size much smaller than the beam diameter *at the center of the*

*scattering cell*, we have to correct the refraction in two directions ( $\Upsilon = 2$ ). When the pinhole size is comparable to the beam diameter,  $1 < \Upsilon < 2$ , which should be avoided. In practice, a slit ( $\sim 200 \mu\text{m}$ ) is preferred. Note that static LLS theory is not complicated, but the alignment of LLS spectrometer is much more difficult.

[\[Top of Page\]](#)

### 3. Dynamic Laser Light Scattering

When the incident light is scattered by a moving particle, the detected frequency of the scattered light will be slightly higher or lower owing to the Doppler effect, depending on whether the particle moves toward or away from the detector. The frequency distribution of the scattered light is slightly broader than that of the incident light. This is why dynamic LLS is also called quasi-elastic light scattering. In comparison with the incident light frequency ( $\sim 10^{15}$  Hz), the frequency broadening  $\Delta f$  approximately  $10^5$ – $10^7$  Hz is so small, that it is difficult, if not impossible, to detect  $\Delta f$  in frequency domain. But, it can be recorded in the time domain via a time correlation function so that dynamic LLS is sometimes known as photon correlation spectroscopy.

Without a local oscillator (ie, a constant fraction of the incident light reaching the detector by various *intentionally or unintentionally* sources, such as surface scratching or reflection), the self-beating of the scattered electric field leads to the intensity-intensity time correlation function,  $G^{(2)}(q, t)$ , which is related to the normalized scattered electric field-electric field time correlation function  $|g^{(1)}(q, t)|$  ( $= \langle \mathbf{E}(q, 0)\mathbf{E}^*(q, t) \rangle / \langle \mathbf{E}(q, 0)\mathbf{E}^*(q, 0) \rangle$ ) by the Siegert relation:

$$G^{(2)}(q, t) = \langle I(q, 0)I(q, t) \rangle = A(1 + \beta |g^{(1)}(q, t)|^2) \quad (6)$$

where  $A (\equiv \langle I(q, 0)I(q, 0) \rangle)$  is the baseline,  $t$  is the delay time,  $\beta$  is a parameter depending on the coherence of the detection optics, and  $I(q, t)$  is the detected scattering intensity or photon counts at time  $t$ , including contributions from both solvent and solute. Therefore,  $I_{\text{solution}}(q, t) = I_{\text{solvent}}(q, t) + I_{\text{solute}}(q, t)$ . Figure 2 shows a typical normalized intensity-intensity time correlation function for thermally sensitive and biocompatible poly(*N*-vinyl-caprolactam) in water at 25 °C.

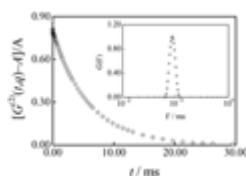


**Figure 2.** Typical normalized intensity-intensity time correlation function for thermally sensitive and biocompatible poly(*N*-vinyl-caprolactam) ( $M_w = 2.34 \times 10^6$  g/mol,  $\langle R_g \rangle = 79$  nm and  $A_2 = 1.59 \times 10^{-4}$  mol mL/g<sup>2</sup>) in water at 25 °C.

In a real experiment,  $\beta_{\text{app}} [= \beta (I_{\text{solute}}/I_{\text{solution}})^2]$  instead of  $\beta$  is measured by the extrapolation of  $[G^{(2)}(q, t)]_{t \rightarrow 0}$  in equation 6 (18). The reader should be aware of this fact, especially for weakly scattered dilute low molar mass polymer solution. For example, if  $I_{\text{solute}} = I_{\text{solvent}}$ ,  $\beta_{\text{app}} = \beta / 4$ . Note that  $\beta$  is a constant for each given detection geometry so that it can be determined by using a strongly scattered object, such as narrowly distributed latex particles ( $\sim 100$  nm). Knowing  $\beta$ , one can calculate  $I_{\text{solute}}$  from  $\beta_{\text{app}}$ . The beginner in LLS should note that such a measurement is not a routine method and only reserved for some particular experiments in which a direct and accurate measurement of  $I_{\text{solution}} - I_{\text{solvent}}$  is

difficult. Generally, the relaxation of  $|g^{(1)}(q,t)|$  includes both diffusion (translation and rotation) and internal motions. Let us first consider the translational diffusion relaxation. For a polydisperse sample with a continuous distribution of molar mass  $M$  or size  $R$ , we have

$$|g^{(1)}(q,t)| = \int_0^\infty G(\Gamma)e^{-\Gamma t} d\Gamma \quad (7)$$

where  $G(\Gamma)$  is the line width distribution. Note that by the definition of  $|g^{(1)}(q,t)|$ ,  $G(\Gamma)$  is an intensity distribution of  $\Gamma$ . For a dilute solution, the measured line width  $\Gamma$  is related to  $q$ ,  $C$ , and the translational diffusion coefficient  $D$  by (19, 20)

$$\Gamma = q^2 D (1 + k_d C) \left( 1 + f \langle R_g^2 \rangle_s q^2 \right) \quad (8)$$

where  $k_d$  is the diffusion second virial coefficient and  $f$  is a dimensionless parameter depending on the structure, internal motions, and solvent. When  $C \rightarrow 0$  and  $q \rightarrow 0$ ,  $\Gamma/q^2 \rightarrow D$ .

Equation 7 indicates that once  $|g^{(1)}(q,t)|$  is determined from  $G^{(2)}(q,t)$  through equation 6,  $G(\Gamma)$  can be computed from the Laplace inversion of  $|g^{(1)}(q,t)|$  (21-27). In the past three decades, many computation programs were developed. At the earlier stage, the calculation speed was a very important factor in the development. This constraint has gradually been removed in the past 10 years. Among many programs, the CONTIN program developed by Provencher (28) is still the most used and accepted one. However, it should be noted that equation 7 is one of the first kind Fredholm integral equations. Its inversion is an ill-conditioned problem because of the bandwidth limitation of photon correlation instruments, unavoidable measurement noises, and a limited number of data points, namely, the inversion does not lead to a unique  $G(\Gamma)$ . Therefore, it is more important to *reduce the noises in the measured intensity time correlation function than to choose a program for data analysis* (27, 28). It is crucial to thoroughly clean (ie, dust-free) the solution. A practical checkup is to measure the scattered intensity at  $15^\circ$  for 5–10 min. If there is no sharp intensity pulse, the sample is “clean.” Unfortunately, many of LLS users did not realize this problem or did not want to face it. It is dangerous to use a “dirty” solution and explain whatever comes from it.

It is worth noting that there is a temptation among LLS users to extract too much information from  $G^{(2)}(q,t)$ , actually from experimental noises. In the literature, three or four peaks in  $G(\Gamma)$  were often reported. It has to be warned that even a bimodal distribution of  $G(\Gamma)$  has to be justified by other physical evidences or preexperimental knowledge. This does not mean that many of the Laplace inversion programs developed in the past are useless. On the contrary, they have been quite successful in retrieving some desired information. Therefore, the Laplace inversion should be used with a clear understanding of its ill-conditioned nature and its limitation.

Berne and Pecora (7) and Russo (14) have discussed the contribution of the rotational relaxation to  $\Gamma$ . At a very small scattering angle, the internal and rotation relaxations are relatively fast that its contribution to  $\Gamma$  can be neglected. The internal motions of a long flexible polymer chain, are also known as the normal modes or “breathing modes,” can only be observed at higher scattering angles. Berne and Pecora (7) and later Perico and co-workers (29) derived the spectral distribution of the light scattered from a flexible polymer chain. Figure 3 shows typical plots of  $G(\Gamma/q^2)$  versus  $\Gamma/q^2$  for a narrowly distributed high molar mass polystyrene standard in

toluene at different  $x$  values (30). The change of  $G(\Gamma/q^2)$  is due to the fact that the line width ( $\Gamma$ ) associated with the translational diffusion increases with  $x$ , but those related to the internal motions are independent of the scattering angle.

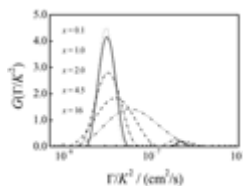


**Figure 3.**  $x$ -dependence of  $G(\Gamma/K^2)$  for a high molar mass polystyrene standard ( $M_w = 1.02 \times 10^7$  g/mol and  $M_w/M_n = 1.17$ ) in toluene at  $T = 20^\circ\text{C}$ , where  $x = (R_g/k)^2$  and  $G(\Gamma/K^2)$  was calculated by using the CONTIN Laplace inversion program.

The uninitiated reader may wish to consult chapters from two books on polydispersity analysis edited by Schulz-DuBois (31) and Dahneke (32). In practice, one can use a fast but limited cumulants analysis to obtain the average line width  $\langle \Gamma \rangle$  and relative width  $\mu_2/\langle \Gamma \rangle^2$  of  $G(\Gamma)$  (21), wherein  $[G^{(2)}(q, t) - A]/A$  is expanded as

$$\ln \left[ \frac{G^{(2)}(q, t) - A}{A} \right] = \ln \beta - \langle \Gamma \rangle t + \frac{\mu_2 t^2}{2!} - \frac{\mu_3 t^3}{3!} + \dots \quad (9)$$

where  $\langle \Gamma \rangle = \int_0^\infty \Gamma G(\Gamma) d\Gamma$  and  $\mu_m = \int_0^\infty (\Gamma - \langle \Gamma \rangle)^m G(\Gamma) d\Gamma$ . For  $\mu_2/\langle \Gamma \rangle^2 < 0.2$ , the second-order cumulants fit is sufficient, whereas when  $\mu_2/\langle \Gamma \rangle^2 \sim 0.2-0.3$ , the third-order cumulants fit is required. For an even higher value of  $\mu_2/\langle \Gamma \rangle^2$ , we cannot simply use a higher order expansion to solve the problem because we do not know how many terms are sufficient to avoid an overfitting of experimental noises. For a broadly distributed samples, the Laplace inversion could yield more reliable  $\langle \Gamma \rangle$  and  $\mu_2/\langle \Gamma \rangle^2$  as long as the measured time correlation function was obtained within a proper bandwidth range and a sufficient photon counts, for example, the baseline has a total counts over  $10^6$ . The Laplace inversion method is particularly useful if  $G(\Gamma)$  is a bimodal distribution where the two peaks are well separated by a factor of 2 or more.

[\[Top of Page\]](#)

## 4. Methods of Combining Static and Dynamic LLS

Dynamic LLS is famous for its application in particle sizing.  $G(\Gamma)$  obtained from a dilute dispersion is converted to the hydrodynamic size distribution  $f(R_h)$  by means of  $D = \Gamma/q^2$  and the Stokes-Einstein relation  $D = k_B T / 6 \pi \eta R_h$  with  $k_B$ ,  $T$ , and  $\eta$  being the Boltzmann constant, the absolute temperature, and solvent viscosity, respectively. All the parameters in the conversion are either well-known constants or precisely measurable by other methods. Therefore, using dynamic LLS to size the particle size distribution is an absolute method without any calibration. Many commercial instruments have been successfully developed on this principle. For details, the reader should refer to the book edited by Gouesbet and Grehan (33). However, a combination of static and dynamic LLS can provide much more than the characterization of the weight average molar mass and the particle size distribution.

### 4.1. Characterization of Molar Mass Distribution

Among other methods, using a combination of static and dynamic LLS to characterize the molar mass distribution of a polymer has yet become popular

because it requires a well-aligned spectrometer which is capable of doing both static and dynamic LLS, a better understanding of LLS theory, and a calibration between  $D$  and  $M$ . It is worth noting that LLS as a nonintrinsic and nondestructive method has its own advantages, for example, it can use a strong corrosive solvent, such as concentrated sulfuric acid, and it can be operated at temperatures as high as 340°C. Although not involving fractionation as in GPC,  $G(\Gamma)$  obtained in dynamic LLS could lead to the molar mass distribution if we have

$$D = k_D M^{-\alpha_D} \quad (10)$$

where  $k_D$  and  $\alpha_D$  are two scaling constants (34). It has been confirmed that for a flexible polymer,  $0.5 < \alpha_D < 0.6$  in a good solvent and  $\alpha_D = 0.5$  in a Flory  $\Theta$ -solvent; for a rigid rod-like chain,  $\alpha_D = 1$ ; and for a semirigid worm-like chain,  $0.6 < \alpha_D < 1$ . Equations 2, 6, and 7 indicate that both  $Mf_w(M)$  and  $G(D)$  are proportional to the excess scattered intensity. Using equation 10, we have (20)

$$f_w(M) \propto D^{1+\frac{2}{\alpha_D}} G(D) \quad (11)$$

Therefore, one can transfer  $D$  to  $M$  and  $f_w(M)$  to  $G(D)$  if knowing  $k_D$  and  $\alpha_D$ , very similar to GPC or the particle sizing where we know that  $k_D = k_B T/6 \pi \eta$  and  $\alpha_D = -1$ . Figure 4 shows such obtained differential weight distributions  $f_w(M)$  of molar mass for four different poly(*N*-vinylcaprolactam) fractions in water at 25°C.

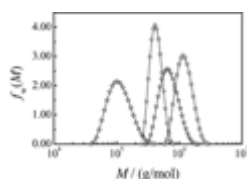


**Figure 4.** Typical differential weight distributions  $f_w(M)$  of molar mass for four different poly(*N*-vinylcaprolactam) fractions in water at 25°C, which were calculated by a combination of static and dynamic LLS results, that is, from the line-width distribution  $G(\Gamma)$  and the weight-average molar mass ( $M_w$ ).

The most straightforward method for calibrating  $D$  versus  $M$  is to measure both  $D$  and  $M$  for a set of narrowly distributed samples with different molar masses (35, 36). However, only a very few kinds of polymers, for example, polystyrene and poly(methyl methacrylate), can be prepared in such a manner. A traditional time-consuming fractionation method has to be used. Hence we often have to satisfy ourselves with one or more broadly distributed samples. For two or more samples, one can determine both  $\alpha_D$  and  $k_D$  from the measure values of  $M_w$  and  $G(D)$  by a method described in Ref. (20). In the case of only one sample, one can estimate  $\alpha_D$  from the Mark-Houwink constant from the calibration between intrinsic viscosity and molar mass, that is,  $[\eta] = k_\eta M_w^{\alpha_\eta}$ . It has been shown that  $\alpha_D \approx (\alpha_\eta + 1)/3$  for a coil chain (34, 37). With  $\alpha_D$  estimated from  $\alpha_\eta$ ,  $M_w$  from static LLS, and  $G(D)$  from dynamic LLS, one can determine  $k_D$  as demonstrated by Chu and co-workers (38, 39) in the characterization of linear polyethylene in 1,2,4-trichlorobenzene at 135°C, where  $\alpha_D$  was estimated from  $\alpha_\eta = 0.72$  reported by Cervenka (40). One can also combine LLS with GPC to find  $\alpha_D$  and  $k_D$  (41, 42). Using a combination of static and dynamic LLS to estimate the molar mass distribution of some special polymers has recently been reviewed (43).

#### 4.2. Estimation of Copolymer Composition Distribution

A copolymer is normally polydisperse not only in molar mass but also in chain composition. A combination of static and dynamic LLS can be used to estimate its

composition distribution. Let us consider a copolymer sample consisting of monomers A and B. We suppose that the copolymer species  $i$  is characterized by the molar mass  $M_i$  and the weight fraction ( $w_A(M_i)$ ). We assume that for a given  $M$ , there is no further composition heterogeneity. For a given copolymer in solvents 1 and 2, we have (44, 45)

$$\frac{f_{w,app}^{(1)}(M)}{f_{w,app}^{(2)}(M)} = \left\{ \frac{\nu^{(2)}w_A(M)\nu_A^{(1)} + [1 - w_A(M)]\nu_B^{(1)}}{\nu^{(1)}w_A(M)\nu_A^{(2)} + [1 - w_A(M)]\nu_B^{(2)}} \right\}^2 \quad (12)$$

where  $f_{w,app}(M)$  is the apparent weight distribution,  $\nu$  is specific refractive index increment, and the superscripts denote two solvents. The values of  $\nu$ ,  $\nu_A$ , and  $\nu_B$  in two solvents can be predetermined using differential refractometer. The ratio on the left-hand side can be determined as a function of  $M$  since  $f_{w,app}(M)$  and  $M_w$  are obtainable using equations 10 and 11. Therefore, equation 12 allows the determination of  $w_A(M)$ . Once  $w_A(M)$  is known, we are ready to compute  $\nu(M)$  and  $f_w(M)$  (44, 45). Figure 5 shows such obtained weight composition for two PET-PCL samples with different weight average molar masses but the same overall composition. It clearly shows that the PET content increases as the molar mass for  $M < \text{approximately } 4 \times 10^4$  and approaches a constant value ( $\sim 14\%$ ) in the high molar mass range.

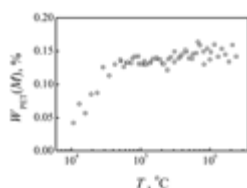


**Figure 5.** Estimate of the chain composition distributions for low mass (o) and high mass (□)13% PET-PCL samples by a combination of static and dynamic LLS.

### 4.3. Investigation of Interchain Aggregation

Using dynamic LLS to size polymer aggregates is only a simple application. A combination of static and dynamic LLS can lead to the weight fraction and molar mass of the aggregates. If a solution contains individual polymer chains and clusters (or aggregates), static LLS can lead to an apparent weight-average molar mass  $M_{w,app} = M_{w,L}w_L + M_{w,H}w_H$ , where the subscripts L and H denote low molar mass polymer chains and high molar mass clusters, respectively, and  $w_L$  and  $w_H$  are their weight fractions with  $w_L + w_H = 1$ . If clusters are much larger than individual chains, dynamic LLS can detect two distinct peaks  $G_L(D)$  and  $G_H(D)$ , as shown in Figure 6 (46). The area ratio  $A_r$  of these two peaks equals the intensity ratio, i.e.,

$$A_r = \frac{A_L}{A_H} = \frac{\int_0^{D_M} G_L(D) dD}{\int_{D_M}^{\infty} G_H(D) dD} = \frac{M_{w,L}x_L}{M_{w,H}x_H} \quad (13)$$

with  $D_M$  being the cutoff translational diffusion coefficient between  $G_L(D)$  and  $G_H(D)$ . Using equations 12 and 13, one can calculate  $M_{w,L}x_L$  and  $M_{w,H}x_H$  from  $M_{w,app}$  and  $A_r$ . With knowing any one of  $M_{w,L}$ ,  $M_{w,H}$ , and  $x_L$  and  $x_H$ , one can find the rest of three. This method has been thoroughly tested (46) and is used to characterize thermoplastic polymers with phenolphthalein in their backbone chains (47).

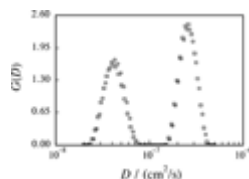


**Figure 6.** Translational diffusion coefficient distributions  $G(D)$  of a simulated polymer mixture at two scattering angles (“o” for  $14^\circ$  and “□” for  $17^\circ$ ). The mixture contains two polystyrene standards of distinctly different weight average molar masses ( $3.0 \times 10^5$  and  $5.9 \times 10^6$  g/mol) and a high mass polystyrene.

#### 4.4. Elucidation of Colloidal Particles

Besides sizing colloidal particles, one can use a combination of static and dynamic LLS to elucidate the structure, density of particles and the adsorbed surfactant or polymer layer, and the particle formation (48-53). The following is just one example of how to determine the particle density ( $\rho$ ) by combining static and dynamic LLS.

For a colloidal particle with a uniform density, its molar mass  $M = (4/3) \pi R^3 \rho N_A$ , where  $R$  is its radius and  $N_A$  is the Avogadro constant.  $D$  can be converted to  $R_h$ . In general,  $R_h \geq R$ , so that one can assume that  $R_h = R + b$  with  $b$  being the thickness of the solvated layer. Thus,

$$D = \frac{1}{1 + b(4\pi\rho N_A/M)^{1/3}} \left( \frac{k_B T}{6\pi\eta} \right) (4\pi\rho N_A)^{1/3} M^{1/3} \quad (14)$$

Comparing equation 14 with equation 10 and considering  $b \ll R$ , one finds approximately  $\alpha = 1/3$  and  $k_D = (k_B T/6\pi\eta)(4\pi\rho N_A)^{1/3}/[1 + b(4\pi\rho N_A/M)^{1/3}]$ .

Replacing  $M$  in equation 14 with  $M_w$ , one has

$$M_w = \frac{1}{[1 + b(4\pi\rho N_A/M_w)^{1/3}]^3} \left( \frac{4\pi\rho N_A}{3} \right) \left( \frac{k_B T}{6\pi\eta} \right)^3 / \int_0^\infty G(D) D^3 dD \quad (15)$$

Equation 15 contains two unknown parameters  $b$  and  $\rho$ . Knowing one of them, one can calculate the other from  $M_w$  and  $G(D)$ . In this way, we found that the polystyrene nanoparticles made of only a few uncrosslinked chains have a slightly lower density than bulk polystyrene or conventional polystyrene latex (54).

#### 4.5. Study of Self-Assembly of Diblock Copolymers

A diblock copolymer can self-assemble into a core-shell nanostructure in a selective solvent in which the core and shell are, respectively, made of the collapsed insoluble blocks and the swollen soluble blocks. For the first approximation, the core-shell nanostructure can be described by two concentric spheres with different, but uniform, densities ( $\rho_c$  and  $\rho_s$ ). Instead of neutron scattering, a combination of static and dynamic LLS can also lead to the core radius ( $R_c$ ) and shell thickness ( $\Delta R$ ) from  $\langle R_g \rangle / \langle R_h \rangle$  by the following principle.

For a sphere with a uniform density, we can write the core and the shell masses ( $M_c$  and  $M_s$ ) as  $M_c = 4\pi\rho_c R_c^3/3$  and  $M_s = 4\pi\rho_s(R^3 - R_c^3)/3$ , where  $R_c$  is the core radius and  $R$  is the particle radius. According to the definition of  $R_g$  for a sphere, we have

$$R_g^2 = \frac{\int_V \rho(r) r^2 dV}{\int_V \rho(r) dV} = \frac{\int_0^{R_c} 4\pi\rho_c r^4 dr + \int_{R_c}^R 4\pi\rho_s r^4 dr}{M_c + M_s} = \frac{3[M_c R_c^2 R^3 - (M_c + M_s) R_c^5 + M_s R^5]}{5(M_c + M_s)(R^3 - R_c^3)} \quad (16)$$

Setting the mass ratio  $M_c/M_s$  as  $A$  and the radius ratio  $R_c/R$  as  $x$ , we can rewrite equation 16 as

$$\frac{R_g}{R_h} = \left\{ \frac{3[Ax^2 - (1+A)x^5 + 1]}{5(1+A)(1-x^3)} \right\}^{1/2} \quad (17)$$

where  $R$  has been replaced with  $R_h$ . Note that  $M_c/M_s$  equals to the molar mass ratio of the insoluble block to the soluble block, a constant for a given diblock copolymer. Therefore, for each measured  $\langle R_g \rangle / \langle R_h \rangle$ , we can find a corresponding  $x$  according to equation 17 and calculate  $R_c$  and  $\Delta R$  since  $R_c = \langle R_h \rangle x$  and  $\Delta R = \langle R_h \rangle - R_c = \langle R_h \rangle (1 - x)$ .

Figure 7 shows a typical average association chain number ( $n_{\text{chain}}$ ) dependence of  $R_c$  and  $\Delta R$  of self-assembled core-shell nanostructures of a rod-coil diblock copolymer. The fact that  $R_c$  is nearly a constant and close to the contour length of the PMPCS block ( $\sim 31$  nm), but  $\Delta R$  increases with  $n_{\text{chain}}$ , clearly reveals that when more copolymer chains are self-assembled into the core-shell nanostructure, the insoluble rod-like PMPCS blocks are simply inserted into the core, whereas the soluble coil-like PS blocks are forced to stretch in the shell due to the repulsion in a good solvent.

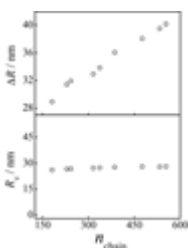


**Figure 7.** Average association chain number dependence of the core radius ( $R_c$ ) and shell thickness ( $\Delta R$ ) of self-assembled core-shell nanostructures of a rod-coil diblock copolymer, poly(styrene-block-(2,5-bis[(5)-methoxyphenyl]oxycarbonyl)styrene) PS-b-PMPCS in *p*-xylene at 25°C.

[\[Top of Page\]](#)

## 5. Practice of Laser Light Scattering

A laser light scattering spectrometer contains a limited number of components: namely, the light source, the optics, the cell holder, and the detector. Nowadays, a LLS instrument should have a digital output (single photon counting) from a fast photomultiplier, that is, the output current pulse have already been treated by preamplifier/amplifier/discriminator before it is connected to a digital time correlator, a single plug-in board to a PC computer.

### 5.1. Light Source

Traditionally, the light source is a helium-neon (He-Ne) laser with a wavelength of 632.8 nm and an output power of 5–50 mW or an argon-ion ( $\text{Ar}^+$ ) laser with a wavelength of 488 or 514.5 nm and an output power of 50–400 mW. Krypton lasers have also been used because their wavelength can be longer than 632.8 nm. The additional cost and somewhat short plasma tube life are drawbacks. The laser used in dynamic light scattering should have a  $\text{TEM}_{00}$  mode with a Gaussian intensity profile. The reader should choose a laser with a beam amplitude RMS noise less than 0.5%. Noted that in dynamic LLS, long-term stability is not very important since the maximum delay time is usually no more than a few minutes, typically less than 1 s, but both the beam point and intensity stabilities are important from static

LLS. Recently, there is a tendency to replace these gas lasers with solid-state CW lasers.

Specially, we like to state that the frequency-doubled Nd-YAG laser (532 nm) is a much better choice nowadays if one does not require two wavelengths. In comparison with gas lasers, the solid laser has the following advantages: (1) its beam diameter is smaller so that small scattering angles are more easier to access; (2) it is approximately ten times more stable; (3) it has a smaller overall size; (4) it is air-cooled and requires only plug-in electric power; and (5) its running cost is lower by a factor of  $\sim 5$  or more. It is expected that solid-state lasers will gradually replace gas lasers in most applications. The manufacturers start to provide a new kind of solid-state CW diode lasers in visible ( $\sim 670$  nm) and near visible (780–830 nm) range, which are particularly useful in the study of conjugated polymers.

## 5.2. Optics and Cell Design

It is well known that laser light follows the Gaussian optics. If a laser beam is focused through an aperture by a lens, the diameter ( $d_s$ ) of the focus spot will be  $\sim 1.22 \lambda f / r_0$  with  $f$  and  $r_0$  being the focal length and beam radius, respectively. If  $r_0 \sim 0.8$  mm,  $\lambda \sim 532$  nm, and  $f \sim 300$  mm, we have a typical  $d_s \sim 0.25$  mm so that the incident beam divergence ( $d_s/f$ ) is less than 1 mrad, sufficiently small. A polarizer may be placed in the light path before the incident beam strikes the sample cell to define the polarization (normally vertical) of the incident beam. Nowadays, the polarization ratio of lasers is better than 100:1 so that the polarizer is not necessary for a normal LLS measurement.

The conventional sample cell holder in LLS consists of a hollow cylindrical brass block with an outside diameter of 50–80 mm and an inside diameter of 10–20 mm, which matches the outside diameter of the scattering cell. The brass block is normally placed inside a cylindrical optical glass cup filled with a fluid (eg, xylene, toluene, and silican oil) whose refractive index matches that of glass ( $\sim 1.5$ ) to reduce the surface scattering and cell curvature. A proper alignment of the optical path requires the variation of the scattered intensity of a standard, benzene or toluene, after the scattering volume correction by  $\sin \theta$  is less than 1% (if the scattering volume is chosen by a slit) or 2% (if a small pinhole is used) over an angular range approximately  $15^\circ$ – $150^\circ$ . In principle, the scattering cell with an optical quality should be used. However, we found in practice that a selected normal cylindrical sample vial is also satisfactory, which reduces the cost and make it disposable.

On the other hand, if one is only interested in dynamic LLS, a rectangular cell can also be used or even preferred. Noted that the scattering volume ( $\sim 200 \times 300 \times 300 \mu\text{m}^3$  or  $0.02 \mu\text{L}$ ) is so small that one can use a small scattering cell, for example, a melting-point capillary with a microliter solution volume for dynamic LLS (65), even though it is difficult to use it in static LLS. The scattering cell can also be a flow type (66) so that it can be used as an *in situ* LLS detector for GPC and electrophoresis. Another challenge in polymer analysis is to characterize polymers soluble only at high temperatures. An important advancement in this direction is the design of a novel light scattering cell holder, which is capable of operating at temperatures as high as  $340^\circ\text{C}$  (67-70). It was first developed at State University of New York at Stony Brook and is now available in DuPont (Experimental Station), BASF (Ludwigshafen, Germany), and our laboratory.

It has to be stated that the optics together with the cell design in LLS are going to a drastic change because of the development of optical fiber technology (73-76).

Figure 8 shows that a fiber-optic detector probe comprising a single mode optical fiber and a graded index microlens that can form an integral part of the scattering cell. In this cell-detector probe design, the probes can eliminate the need for a goniometer, which is often one of the bulkier components of the spectrometer. Moreover, the probe can be in contact with the solution or dispersion so that the requirement of a transparent window in the sample chamber can be relaxed.

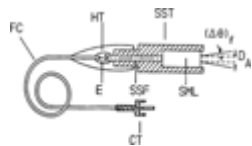


**Figure 8.** Schematic of a typical fiber-optic probe. SST: A matching piece of cylindrical stainless steel; SML: SELFOC microlens; SSF: a stainless steel or ceramic ferrule used for mounting the bare optical fiber; E: epoxy used for holding fiber in ferrule; HT: heat shrink tubing; FC: fiber cable; CT: SMA type II male connector.  $D_A$  and  $\Delta\theta$  are the effective detector aperture and divergence angle, respectively.

### 5.3. Detectors and Detection

Commercially available standard photomultiplier tubes (PMT) with a low dark count (<30 Hz) and a short after-pulsing are normally used to count photons. When a He-Ne laser light source is used, a S-20 photocathode is preferable because of its higher sensitivity in the red range. PMTs, such as EMI 9863 and new Hamamatsu miniature PMTs, are more suitable. To reduce dark count, the PMT with a relatively smaller photocathode (typically 2.54 mm in diameter) should be used. If the laser light is in the blue and green range, PMTs with a bi-alkali photocathode is more adequate because it has a lower dark count at room temperature. The selected EMI 9893 PMT with a low dark count and a short after-pulsing has been popular for this purpose. The RCA C31034 PMT with a broad spectral response (300–800 nm) is good for the entire visible range, but it is more delicate and expensive. The silicon avalanche photodiode (SAP) is another new development and promising in making a miniature light scattering apparatuses. With a broad spectral response, SAPs are matched to diode lasers to simplify the LLS instrumentation, especially if it is combined with a fiber-optic probe, as recently demonstrated by ALV (Germany).

Figure 9 shows two commonly used configurations of the detection optics. In static LLS, the first pinhole (P1) can be replaced by a slit so that the alignment will be easier but it has to be switched back to a pinhole for dynamic LLS, which makes a simultaneous static and dynamic measurement impossible. In A-configuration, the scattering volume is mainly determined by the diameter ( $d_{P1}$ ) of P1 (or the slit width). The first pinhole should be as close as possible to the cell, so that the scattering volume will be better defined. However, owing to the existence of the cell holder and index-matching cup, the first pinhole is normally 10–15 cm away from the scattering center. The second pinhole is located exactly on the focal plane of the lens and the opening angle of  $d_{P2}/f$  determines the uncertainty of the scattering angle ( $\Delta\theta$ ). The coherent factor ( $\beta$ ) in equation 6 is mainly determined by the opening angle of  $d_{P2}/L_0$  but also influenced by  $d_{P1}$ . In this design, the alignment will be easier and the distance between the cell and the detector could be smaller. In practice,  $f \sim 10$  cm,  $L_0 \sim 10$  cm,  $d_{P1}$  approximately 200–400  $\mu\text{m}$ , and  $d_{P2}$  approximately 100–200  $\mu\text{m}$ .

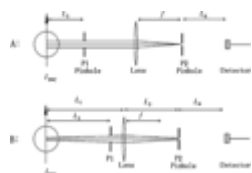


**Figure 9.** Two commonly used configurations of the detection optics for both static and dynamic laser light scattering, where  $I_{INC}$  is the incident light and  $f$  is the focal length.

In B-configuration,  $L_1$ ,  $L_2$ , and  $f$  are related by  $1/L_1 + 1/L_2 = 1/f$ , that is, the scattering center and the second pinhole are located exactly on the imaging planes of the lens. The scattering volume is precisely determined by  $d_{P2}$ .  $\Delta \theta$  is determined by the opening angle of  $d_{P1}/L_3$ . Therefore, the first pinhole should be placed as close as possible to the lens, which has no difficulty in practice. If  $L_1 = L_2 = 2f$ , that is, the so-called  $2f$ - $2f$  configuration, the second pinhole is optically moved to the scattering center.  $\beta$  is still determined by the opening angle of  $d_{P2}/L_0$ . In this configuration,  $f$  approximately 5–10 cm, smaller than the previous one. For a given  $d_{P2}$ , the scattering volume can be enlarged by a factor of  $L_1/L_2$  (normally,  $L_1/L_2 \leq 3$ ), so that one can simultaneously have a stronger scattering intensity, a higher  $\beta$ , and a smaller  $\Delta \theta$  for a given distance between the scattering center and the detector. However, the alignment is more difficult but manageable.

#### 5.4. Sample Preparation

If a polymer can be dissolved in more than one solvent, the choice of solvent for LLS should be made generally according to the following guidelines: (1) colorless to avoid the absorption; (2) a higher contrast, that is, a higher  $dn/dC$ ; and (3) less polar and less viscous to make the dust-free easier. In practice, we may have no choice. For example, poly(1,4-phenyleneterephthalamide) (PPTA or Kevlar) is only soluble in very strong and viscous acids. In such a case, ultracentrifugation instead of filtration has to be used (17, 77). As for a copolymer, the selection of proper solvents is even more difficult because at least two solvents, which satisfy the three guidelines, are needed. For this reason, only a few works related to the copolymer characterization have been reported so far (78-81). As for polymers only soluble at high temperatures, the preparation of a polymer solution for LLS is a challenge. Finding a solvent with a high boiling point is often not easy, but the dissolution and clarification at high temperatures are even more difficult. Two novel high temperature dissolution-and-filtration apparatuses have been developed (67, 70).

#### 5.5. Differential Refractometer

One of the most important parameters in static LLS is the specific refractive index increment ( $dn/dC$ ), which is defined as  $\lim_{C \rightarrow 0} (\partial n / \partial C)_{T,P,\lambda}$ . equation 2 shows that an error of  $E\%$  in  $dn/dC$  will lead to an error of  $2E\%$  in  $M_w$ . The refractive index increment  $\Delta n$  of a polymer solution is usually measured using either a differential refractometer or an interferometer. In a differential refractometer, the light beam is refracted at the boundary between solution and solvent. Commonly, the beam displacement is directly measured and then converted to  $\Delta n$  after multiplying a calibration constant. The refractometer is normally calibrated by using a solution with an accurately known refractive index difference  $\Delta n$  (82, 83). This is not an absolute method since the constant has to be calibrated at the same conditions as those used in LLS. In an interferometer, two light beams with identical geometrical paths passed two different optical paths. One passes through solution and the other passes solvent. This method relies on the interference of the two beams. Its detail can be found elsewhere (84, 85). In a high temperature LLS measurement, the conventional divided differential refractometer cuvette has to be replaced by a deformed cylindrical light scattering cell in which the laser beam  $\lambda$  is refracted by the solution/air interface (68).

Figure 10a schematically shows a novel differential refractometer, which was first designed by Wu and co-workers (86, 87) and later commercialized by Jianke Instrument Co. Ltd (Anhui, People's Republic of China). A small pinhole with a diameter of 200–400  $\mu\text{m}$  is illuminated with a laser light. The illuminated pinhole is

imaged to a position-sensitive detector (PSD) (Hamamatsu S3931) by a lens located at an equal distance from the pinhole and the detector. The focal length ( $f$ ) of the lens  $f$  is 200 mm. This refractometer adopted a ( $2f-2f$ ) design. Note that in a conventional ( $1f$ ) design, a parallel incident light beam is used and the distance between the detector and the lens is only one focal length. The conventional design cannot solve the beam drift problem associated with a laser. A temperature-controlled refractometer cuvette (Hellma 590.049-QS) is placed just in front of the lens. It is a flow cell divided into two compartments with a volume of  $\sim 20 \mu\text{L}$ . All the components are rigidly mounted on a flat metal board and sealed with side and top shells as a box. The output voltage ( $-10$  to  $10$  V) from the position-sensitive detector is proportional to the displacement of the light spot from the center of the detector and can be measured by a digital voltmeter or an analogue-to-digital data acquisition system and a personal computer. Figure 10b shows the basic principle and the light path of the refractometer, where  $\theta_1$ ,  $\theta_2$ ,  $\theta_3$ , and the cuvette are drawn enlarged to make the details clear. It can be shown that  $\Delta x = K \Delta n$ , where  $K = [X + c(1 - 1/n_0)] \tan(90^\circ - \theta)$ . For a given optical setup and solvent,  $X$ ,  $c$ ,  $\theta$ ,  $n_0$ , and hence  $K$  are constants. Therefore, the signal is proportional to  $\Delta n$ . This ( $2f-2f$ ) design is optically equivalent to placing the detector directly behind the pinhole, so that the beam drift problem is solved. The developed refractometer has been incorporated into commercial LLS (86) to measure the ( $dn/dc$ ) in which the laser and computer are shared. Moreover, it has also been independently used to *in situ* study the enzymatic degradation kinetics of some bionanoparticles by monitoring the change of the refractive index (87).

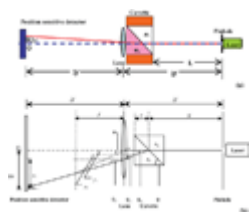


**Figure 10.** (a) Schematic view of a novel differential refractometer (commercialized by Jianke Instrument Co. Ltd, Anhui, People's Republic of China), which consists of a pinhole, a differential refractometer cuvette, a lens ( $f = 20$  cm), and a PSD. All components are rigidly mounted on a long metal board ( $\sim 100$  cm). (b) Light path in which one compartment of the cuvette contains a solvent with refractive index  $n$ , and the other contains a solution with slightly different refractive index  $n = n_0 + \Delta n$ . The cuvette and angles  $\theta'$ ,  $\theta''$  and  $\theta'''$  (actually very small,  $\sim 0.01$  radian) are enlarged to make the light path distinct.

On the basis of the original  $2f-2f$  optical design, we have recently further modified the differential refractometer to be portable by placing a combination of a convex lens and a laser mirror just after the divided cells. Figure 11 showed the details of this portable differential refractometer. The lens just after the cuvette was replaced by a combination of a convex lens (Melles Griot 01LDX347, focal length = 350 mm) and a laser mirror (Edmund, diameter = 25 mm). The convex lens is tightly clung to the laser mirror, and we can assume no gap existence between them. This combination of the lens and mirror therefore has the same functions as two equal lens positions along the optical axis. The laser beam is incident on the sample cuvette, passes through the lens, and then reflected back by the mirror. In this way, the beams after passing through the 50/50 beam splitter and the cuvette, undergo a double reflection before they are reflected to the PSD. The optical path length between the detector and the pinhole is now only two times of the focal length of lens instead of four times as shown in Figure 10. Therefore, the dimension of the instrument can be significantly reduced. It should be note that the combination of two same focal length of the thin lenses without gap is equivalent to a single lens with a focal length half of the thin lens, that is,  $f/2$ . For two ideal thin lenses have the same focal length ( $f$ ) and assume that there is no gap between them, the Gaussian equation in geometry optics is expressed as

$$\frac{1}{u_1} + \frac{1}{v_1} = \frac{1}{f}$$

$$\frac{1}{u_2} + \frac{1}{v_2} = \frac{1}{f}$$
(18)

where  $u$  and  $v$  are the objective and image distance of the lenses, respectively. For two closely combined lenses,  $u_2 = -v_1$ , equation 18 can be rewritten as

$$\frac{1}{u_1} + \frac{1}{v_2} = \frac{1}{(f/2)}$$
(19)

Therefore, we can conclude that the placing closely the combination of a lens ( $f = 350$  mm) and a mirror just after the cuvette is equivalent to one lens with  $f = 175$  mm placing at the same position. On the other hand, the  $2f$ - $2f$  design is maintained by placing both the laser pinhole and detector 350 mm away from the combination unit.

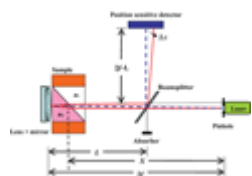


**Figure 11.** Schematic view of a novel portable differential refractometer, which was a further modified version of Figure 10 by placing a combination of a convex lens (focal length =  $2f = 350$  mm) and a laser mirror just after the divided cells and addition of a beam splitter ( $L = 180 \pm 1$  mm)

In this manner, when the laser beam passes through the cuvette, it will undergo a double reflection but keep the  $2f$ - $2f$  configuration. The returned beam is then reflected by a beam splitter to the position sensitive detector. One advantage of this modification is that in comparison to the former design, the optical path distance between the detector and pinhole is reduced from four times of the focal length of the lens to two times. Therefore, the dimensions of the instrument are significantly saved and the modified refractometer can be compact and portable. On the other hand, the precision of the measured  $\Delta n$  is close to  $\sim 10^{-6}$  RI unit, for example, which corresponds to a polymer concentration change as small as  $\sim 10^{-5}$  g/mL. By considering that more and more analysis in industry and also academic researches need dynamic and rapid measurements, such a portable refractometer is particularly attractive. After modification, the refractometer has outer dimensions of only 50 cm in length, 33 cm in width, and 17 cm in height.

## 5.6. Portable Particle Sizer

Based on the dynamic light scattering principle, portable particle sizer, a novel size analyser was designed by Wu and co-workers and commercialized by Jianke Instrument Co. Ltd (Anhui, People's Republic of China). It is an ultrafast and easy-operating size analyzer for industry and research, which can be widely applied to detect size and size distribution of polymer, protein, nanoparticles, surfactants, or emulsion systems ranging from 10 to 1000 nm with controllable temperature range from 10.0 to 50.0 °C ( $\pm 0.1$  °C).

Jianke portable particle sizer offers light scattering measurements at three different scattering angles around 30° (position 1), 90° (position 2), and 150° (position 3) by introducing a novel optical fiber coupling design, which successfully replaced the heavy goniometer. In this manner, the outer dimension of this instrument is only 45 cm in length, 14 cm in width, and 16 cm in height so it is portable and compact. Fast photon counting head (Hamamatsu H8259, Japan) and specialized data processing card (Jianke Instrument Co. Ltd, Anhui, People's Republic of China)

was employed to guarantee synchronous monitor of the real-time scattered intensity fluctuation. By analysis, the time autocorrelation function of the intensity with delay time  $\tau$  ranging from 16  $\mu\text{s}$  to 589 ms, the measured line width  $\Gamma$  can be obtained according equations 6 and 7. For diluted solution,  $\Gamma$  has a simple relationship with scattering wave vector  $q$  and translational diffusion coefficient  $D$ :  $\Gamma = Dq^2$ , where  $q = 4\pi n \sin(\theta)/\lambda$ , where  $n$  is refractive index of the solvent,  $\theta$  is a scattering angle, and  $\lambda$  is wave length. A typical diagram of the normalized intensity-intensity time correlation function and the dependence of  $\Gamma$  and  $q^2$  for polystyrene nanoparticles dispersed in D.I. water are shown in Figure 12, where positions 1, 2 and 3 corresponded to 30.5°, 93.1°, and 127.0°, respectively, which were calibrated by ALV Laser Light Scattering 5000.  $D$  can be obtained by means of  $D = \Gamma/q^2$ . Meanwhile,  $G(\Gamma)$  obtained from a dilute dispersion could be converted to the hydrodynamic size distribution  $f(R_h)$  by the Stokes-Einstein relation  $D = k_B T / 6\pi\eta R_h$ . All the parameters in the conversion are either well-known constants or precisely measurable by other methods.

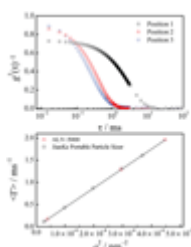


**Figure 12.** Top: The normalized intensity-intensity time correlation function  $g^2(\tau) - 1$  via  $\tau$  from 16  $\mu\text{s}$  to 589 ms measured by portable particle sizer; Bottom: Dependence of  $\Gamma$  and  $q^2$  for polystyrene nanoparticles dispersed in D.I. water at 25.0°C.

[\[Top of Page\]](#)

## Bibliography

1. [book](#) B. Chu, *Laser Light Scattering*, 2nd ed., Academic Press, New York, 1991.
2. [book](#) M. B. Huglin, *Light Scattering from Polymer Solution*, Academic Press, New York, 1972.
3. M. B. Huglin, *Top. Curr. Chem.* **73**, 141 (1977). [Links](#)
4. [book](#) O. Glatter and O. Kratky, *Small-Angle X-ray Scattering*, Academic Press, New York, 1982.
5. S. B. Dubin, N. A. Clark, and G. B. Benedek, *J. Chem. Phys.* **54**, 5158 (1971). [Links](#)
6. [book](#) G. D. Patterson, *Methods of Experimental Physics*, Vol. **16A**, Academic Press, New York, 1980, pp. 170–204.
7. [book](#) B. J. Berne and R. Pecora, *Dynamic Light Scattering*, John Wiley & Sons, New York, 1976.
8. B. H. Zimm, *J. Chem. Phys.* **16**, 1093 (1948). [Links](#)
9. S. Chandrasekhar, *Rev. Mod. Phys.* **15**, 1 (1943). [Links](#)
10. [book](#) P. Munk, *Introduction to Macromolecular Science*, John Wiley & Sons, New York, 1989, p. 255.
11. P. Debye, *J. Phys. Coll. Chem.* **51**, 18 (1947). [Links](#)
12. B. H. Zimm, *J. Chem. Phys.* **16**, 1100 (1948). [Links](#)
13. A. C. W. Lau and C. Wu, *Macromolecules* **32**, 581 (1999). [Links](#)
14. [book](#) P. S. Russo, in W. Brown, ed., *Dynamic Light Scattering*, Oxford University Press, New York, 1993, Chap. 12.

15. B. Chu, Q. Ying, C. Wu, and J. Ford, *Polym. Commun.* **25**, 211 (1984). [Links](#)
16. B. Chu, Q. Ying, and C. Wu, *Polymer* **26**, 1408 (1985). [Links](#)
17. Q. Ying and B. Chu, *Die Makromol. Chem., Rapid Commun.* **5**, 785 (1984). [Links](#)
18. S. T. Sun, I. Nishio, G. Swislow, and T. Tanaka, *J. Chem. Phys.* **73**, 5971 (1980). [Links](#)
19. W. H. Stockmayer and M. Schmidt, *Macromolecules* **17**, 509 (1984). [Links](#)
20. C. Wu, S. Q. Zhou, and W. Wang, *Biopolymer* **35**, 385 (1995). [Links](#)
21. D. E. Koppel, *J. Chem. Phys.* **57**, 4814 (1972). [Links](#)
22. A. K. Livesey, P. Licinio, and M. Delaye, *J. Chem. Phys.* **84**, 5102 (1986). [Links](#)
23. J. G. McWhirter and E. R. Pike, *J. Phys. A* **11**, 1729 (1978). [Links](#)
24. B. Chu, J. R. Ford, and H. S. Dhadwal, *Methods Enzymol.* **117**, 256 (1983). [Links](#)
25. B. Chu, C. Wu, and J. R. Ford, *J. Colloid Interface Sci.* **105**, 473 (1985). [Links](#)
26. J. Raczek, *Eur. Polym. J.* **19**, 607 (1983). [Links](#)
27. E. Nordmeier and M. D. Lechner, *Polym. J.* **21**, 623 (1989). [Links](#)
28. S. W. Provencher, *J. Chem. Phys.* **64** (7), 2772 (1976). [Links](#)
29. A. Perico, P. Piaggio, and C. Cuniberti, *J. Chem. Phys.* **62** (7), 2690 (1975). [Links](#)
30. C. Wu, K. K. Chan, and K. Q. Xia, *Macromolecules* **28**, 1032 (1995). [Links](#)
31. **book** E. Q. Schulz-DuBois, ed., *Proceedings of the 5th International Conference on Photon Correlation Techniques in Fluid Mechanics*, Springer-Verlag, New York, 1983.
32. **book** B. E. Dahneke, ed., *Measurements of Suspended Particles by Quasi-elastic Light Scattering*, John Wiley & Sons, New York, 1983.
33. **book** G. Gouesbet and G. Grehan, *Optical Particle Sizing*, Plenum Press, New York, 1988.
34. **book** P. G. de Gennes, *Scaling Concepts in Polymer Physics*, Cornell University Press, Ithaca, N.Y., 1979.
35. B. Appelt and G. Meyerhoff, *Macromolecules* **13**, 657 (1980). [Links](#)
36. C. Wu, Y. B. Zhang, X. H. Yan, and R. S. Cheng, *Acta Polym Sin* **3**, 349 (1995). [Links](#)
37. **book** P. J. Flory, *Principles of Polymer Chemistry*, Cornell University Press, Ithaca, N.Y., 1953.
38. B. Chu, M. Onclin, and J. R. Ford, *J. Phys. Chem.* **88**, 6566 (1984). [Links](#)
39. J. Pope and B. Chu, *Macromolecules* **17**, 2633 (1984). [Links](#)
40. A. Cervenka, *Makromol. Chem.* **170**, 239 (1973). [Links](#)
41. C. Wu, *Macromolecules* **26**, 5423 (1993). [Links](#)
42. C. Wu, *J. Polym. Sci., Polym. Phys. Ed.* **32**, 803 (1994). [Links](#)
43. C. Wu, *Adv. Polym. Sci.* **137**, 103 (1998). [Links](#)
44. C. Wu, D. Ma, X. Luo, K. K. Chan, and K. F. Woo, *J. Appl. Polym. Sci.* **53**, 1323 (1994). [Links](#)
45. C. Wu, K. F. Woo, X. Luo, and D. Ma, *Macromolecules* **27**, 6055 (1994). [Links](#)
46. C. Wu, M. Siddiq, and K. F. Woo, *Macromolecules* **28**, 4914 (1995). [Links](#)
47. C. Wu, M. Siddiq, and S. Q. Bo, *Macromolecules* **29**, 2989–3157 (1996). [Links](#)
48. M. Li, M. Jiang, and C. Wu, *Macromolecules* **30**, 2201 (1997). [Links](#)

49. C. Wu, *Macromolecules* **27**, 7099 (1994). [Links](#)
50. C. Wu, M. Chen, and M. Akashi, *Macromolecules* **30**, 2187 (1997). [Links](#)
51. J. Gao, S. Q. Zhou, and C. Wu, *Polym. Eng. Sci.* **36**, 2968 (1996). [Links](#)
52. C. Wu, and K. K. Chan, *J. Polym. Sci., Polym. Phys., Ed.*, **33** 919 (1994). [Links](#)
53. C. Wu, R. Y. Qian, and D. H. Napper, *Macromolecules* **28**, 1592 (1994). [Links](#)
54. C. Wu, R. Y. Qian, and D. H. Napper, *Macromolecules* **28**, 1592 (1995). [Links](#)
55. I. Nishio, J. C. Reina, and R. Bansil, *Phys. Rev. Lett.* **59**, 684 (1987). [Links](#)
56. P. N. Pusey and W. van Megen, *Physica A* **157**, 705 (1989). [Links](#)
57. P. Debye and A. M. Bueche, *J. Appl. Phys.* **20**, 518 (1949). [Links](#)
58. C. Wu, J. Zuo, and B. Chu, *Macromolecules* **22**, 838 (1989). [Links](#)
59. C. Wu, J. Zuo, and B. Chu, *Macromolecules* **22**, 633 (1989). [Links](#)
60. M. Shibayama, *Macromol. Chem. Phys.* **199**, 1, (1998). [Links](#)
61. S. Kobayasi, *Rev. Sci. Instrum.* **56**, 160 (1985). [Links](#)
62. C. Allain, M. Drifford, and B. Gauthier-Manuel, *Polymer* **27**, 177 (1986). [Links](#)
63. J. G. H. Joosten, J. L. McCarthy, and P. N. Pusey, *Macromolecules* **24**, 6690 (1991). [Links](#)
64. L. Fang and W. Brown, *Macromolecules* **25**, 6897 (1992). [Links](#)
65. R. Foord, E. Jakeman, C. J. Oliver, E. R. Pike, and co-workers. *Nature* **277**, 242 (1970). [Links](#)
66. B. Chu, R. Xu, T. Maeda, and H. S. Dhadwal, *Rev. Sci. Instrum.* **59**, 716 (1988). [Links](#)
67. C., Wu, W. Buck, and B. Chu, *Macromolecules* **20**, 98 (1987). [Links](#)
68. B. Chu and C. Wu, *Macromolecules* **20**, 93 (1987). [Links](#)
69. B. Chu, C. Wu, and J. Zuo, *Macromolecules* **20**, 700 (1987). [Links](#)
70. B. Chu, C. Wu, and W. Buck, *Macromolecules* **21**, 397 (1988). [Links](#)
71. B. Chu, C. Wu, and W. Buck, *Macromolecules* **22**, 831 (1989). [Links](#)
72. C. Wu, *Makromol. Chem., Makromol. Symp.* **61**, 377 (1992). [Links](#)
73. R. G. Brown, *Appl. Opt.* **26**, 4846 (1987). [Links](#)
74. R. G. Brown and A. P. Jackson, *J. Phys. E* **20**, 1503. [Links](#)
75. H. S. Dhadwal and B. Chu, *Rev. Sci. Instrum.* **60**, 845 (1989). [Links](#)
76. H. S., Dhadwal, C. Wu, and B. Chu, *Appl. Opt.* **28**, 4199 (1989). [Links](#)
77. B. Chu, C. Wu, and J. Ford, *J. Colloid Interface Sci.* **105**, 473 (1985). [Links](#)
78. W. Bushuk and H. Benoit, *Can. J. Chem.* **36**, 1616 (1958). [Links](#)
79. B. Chu, Q. Ying, D. C. Lee, and D. Q. Wu *Macromolecules* **18**, 1962 (1985) [Links](#)
80. W. H. Stockmayer, L. D. Moore, M. Fixman, and B. N. Epstein, *J. Polym. Sci.* **16**, 517 (1955). [Links](#)
81. C. Wu, K. F. Woo, X. L. Luo, and D. Z. Ma, *Macromolecules* **27**, 6055 (1994). [Links](#)
82. M. Obasa, H. Nakamura, M. Takasaka, T. Keto, and M. Nagasawa, *Polym. J.* **25**, 301 (1993). [Links](#)
83. **other** Application Notes LS7. Chromatix, Mountain View, Calif.
84. I. Baltog, C. Ghita, and L. Ghita, *Eur. Polym. J.* **6**, 1299 (1970). [Links](#)
85. **other** Application Notes Optilab 903, Wyatt Technology, Santa Barbara, Calif.
86. C. Wu, and K. Q. Xia, *Rev. Sci. Instrum.* **65**, 587 (1994). [Links](#)
87. H. F. Lam, X. J. Gong, and C. Wu, *J. Phys. Chem. B* **111**, 1531 (2007). [Links](#)

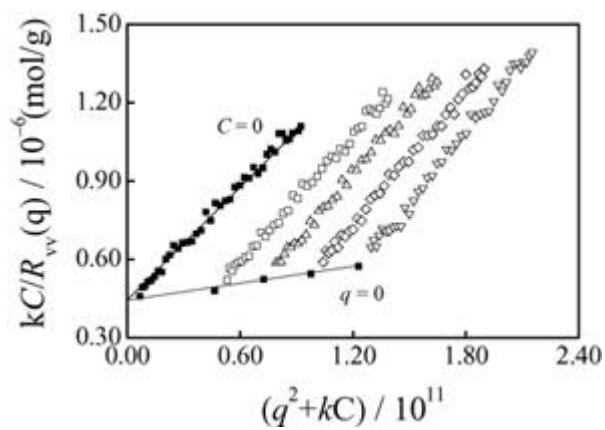
[\[Top of Page\]](#)

[About Wiley InterScience](#) | [About Wiley](#) | [Privacy](#) | [Terms & Conditions](#)  
[Copyright](#) © 1999-2009 [John Wiley & Sons, Inc.](#) All Rights Reserved.

## Laser Light Scattering: Some Recent Developments

[Print](#) | [Close Window](#)

**Figure 1.** Typical Zimm plot for thermally sensitive and biocompatible poly(*N*-vinyl-caprolactam) ( $M_w = 2.34 \times 10^6$  g/mol,  $R_g = 79$  nm and  $A_2 = 1.59 \times 10^{-4}$  mol mL/g<sup>2</sup>) in water at 25 °C.



*Encyclopedia of Polymer Science and Technology*  
Published by John Wiley & Sons, Inc.

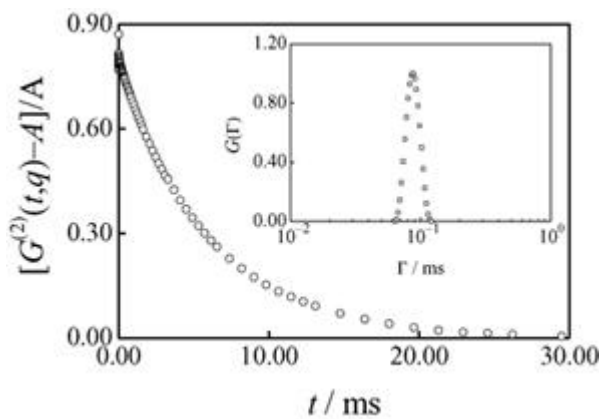
[Print](#) | [Close Window](#)

 Wiley InterScience Logo

## Laser Light Scattering: Some Recent Developments

[Print](#) | [Close Window](#)

**Figure 2.** Typical normalized intensity-intensity time correlation function for thermally sensitive and biocompatible poly(*N*-vinyl-caprolactam) ( $M_w = 2.34 \times 10^6$  g/mol,  $R_g = 79$  nm and  $A_2 = 1.59 \times 10^{-4}$  mol mL/g<sup>2</sup>) in water at 25°C.



Encyclopedia of Polymer Science and Technology  
Published by John Wiley & Sons, Inc.

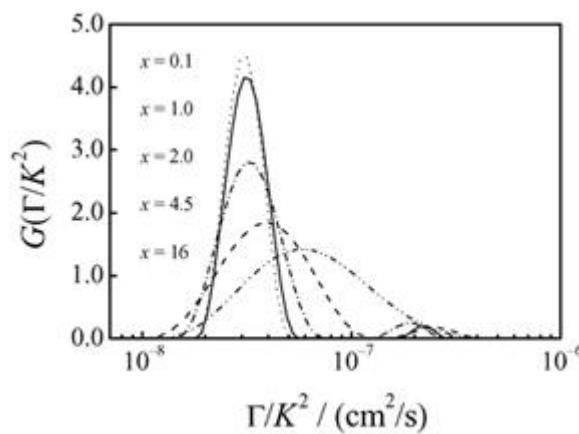
[Print](#) | [Close Window](#)

 Wiley InterScience Logo

## Laser Light Scattering: Some Recent Developments

[Print](#) | [Close Window](#)

**Figure 3.**  $x$ -dependence of  $G(\Gamma/K^2)$  for a high molar mass polystyrene standard ( $M_w = 1.02 \times 10^7$  g/mol and  $M_w/M_n = 1.17$ ) in toluene at  $T = 20^\circ\text{C}$ , where  $x = (R_g K)^2$  and  $G(\Gamma/K^2)$  was calculated by using the CONTIN Laplace inversion program.



Encyclopedia of Polymer Science and Technology  
Published by John Wiley & Sons, Inc.

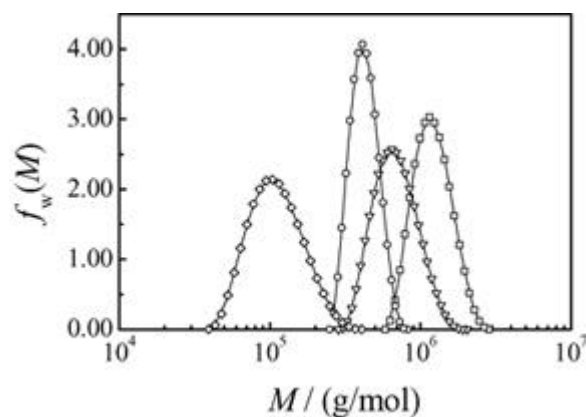
[Print](#) | [Close Window](#)

 Wiley InterScience Logo

## Laser Light Scattering: Some Recent Developments

[Print](#) | [Close Window](#)

**Figure 4.** Typical differential weight distributions  $f_w(M)$  of molar mass for four different poly(*N*-vinylcaprolactam) fractions in water at 25°C, which were calculated by a combination of static and dynamic LLS results, that is, from the line-width distribution  $G(\Gamma)$  and the weight-average molar mass ( $M_w$ ).



*Encyclopedia of Polymer Science and Technology*  
Published by John Wiley & Sons, Inc.

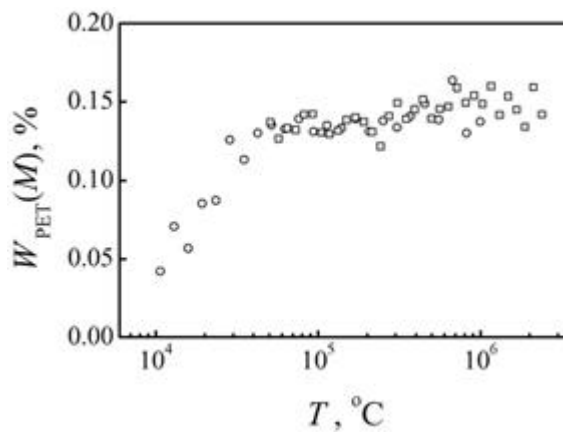
[Print](#) | [Close Window](#)

 Wiley InterScience Logo

## Laser Light Scattering: Some Recent Developments

[Print](#) | [Close Window](#)

**Figure 5.** Estimate of the chain composition distributions for low mass (o) and high mass (□)13% PET-PCL samples by a combination of static and dynamic LLS.



Encyclopedia of Polymer Science and Technology  
Published by John Wiley & Sons, Inc.

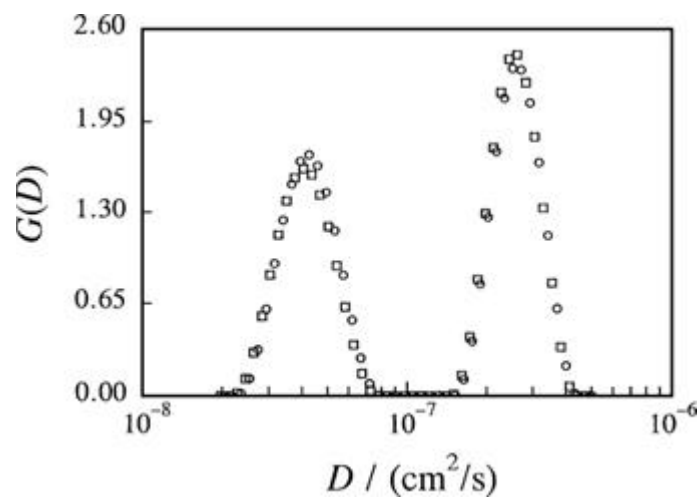
[Print](#) | [Close Window](#)

 Wiley InterScience Logo

## Laser Light Scattering: Some Recent Developments

[Print](#) | [Close Window](#)

**Figure 6.** Translational diffusion coefficient distributions  $G(D)$  of a simulated polymer mixture at two scattering angles ("o" for  $14^\circ$  and "□" for  $17^\circ$ ). The mixture contains two polystyrene standards of distinctly different weight average molar masses ( $3.0 \times 10^5$  and  $5.9 \times 10^6$  g/mol) and a high mass polystyrene.



Encyclopedia of Polymer Science and Technology  
Published by John Wiley & Sons, Inc.

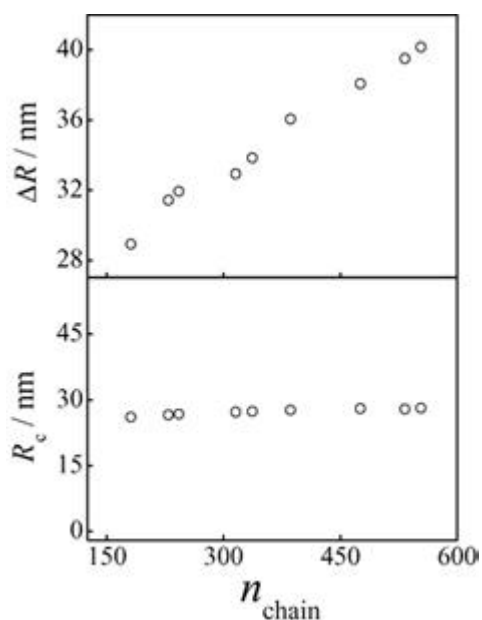
[Print](#) | [Close Window](#)

 Wiley InterScience Logo

## Laser Light Scattering: Some Recent Developments

[Print](#) | [Close Window](#)

**Figure 7.** Average association chain number dependence of the core radius ( $R_c$ ) and shell thickness ( $\Delta R_h$ ) of self-assembled core-shell nanostructures of a rod-coil diblock copolymer, poly(styrene-block-(2,5-bis[(5)-methoxyphenyl]oxycarbonyl)styrene) PS-*b*-PMPCS in *p*-xylene at 25°C.



*Encyclopedia of Polymer Science and Technology*  
Published by John Wiley & Sons, Inc.

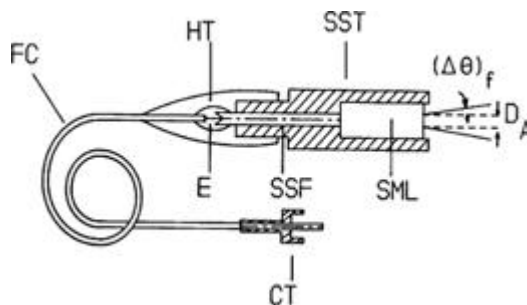
[Print](#) | [Close Window](#)

 Wiley InterScience Logo

## Laser Light Scattering: Some Recent Developments

[Print](#) | [Close Window](#)

**Figure 8.** Schematic of a typical fiber-optic probe. SST: A matching piece of cylindrical stainless steel; SML: SELFOC microlens; SSF: a stainless steel or ceramic ferrule used for mounting the bare optical fiber; E: epoxy used for holding fiber in ferrule; HT: heat shrink tubing; FC: fiber cable; CT: SMA type II male connector.  $D_A$  and  $\Delta\theta$  are the effective detector aperture and divergence angle, respectively.



*Encyclopedia of Polymer Science and Technology*  
Published by John Wiley & Sons, Inc.

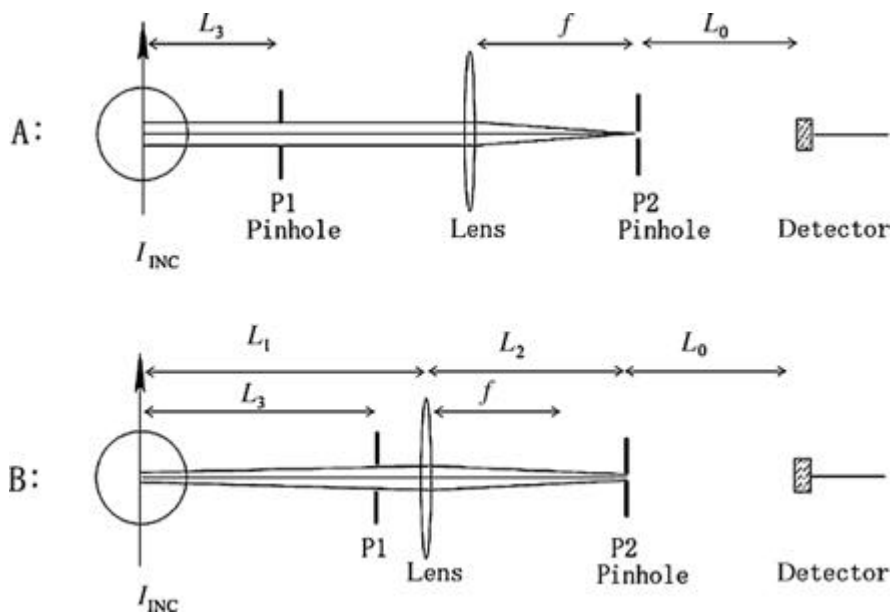
[Print](#) | [Close Window](#)

 Wiley InterScience Logo

## Laser Light Scattering: Some Recent Developments

[Print](#) | [Close Window](#)

**Figure 9.** Two commonly used configurations of the detection optics for both static and dynamic laser light scattering, where  $I_{INC}$  is the incident light and  $f$  is the focal length.



Encyclopedia of Polymer Science and Technology  
Published by John Wiley & Sons, Inc.

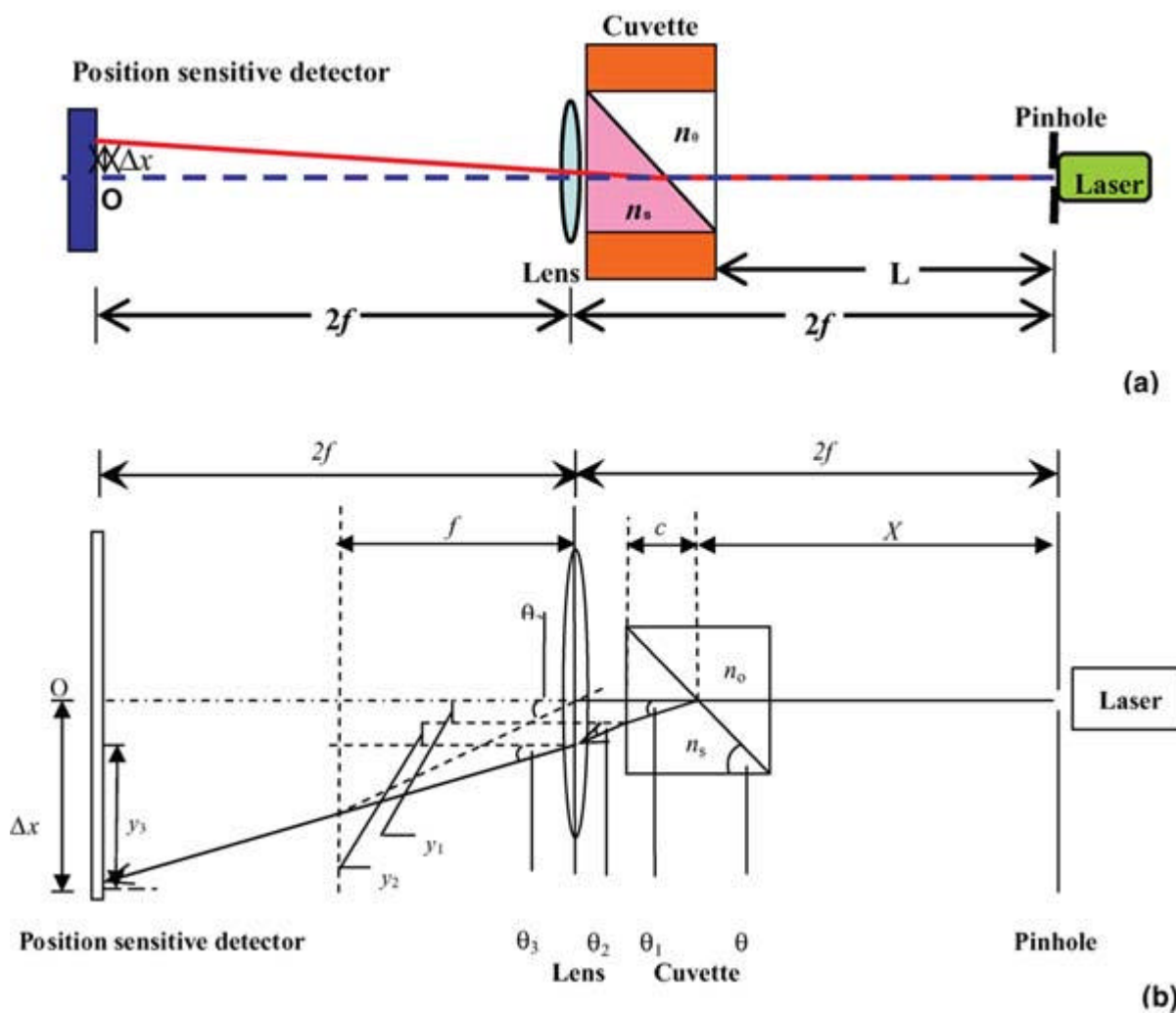
[Print](#) | [Close Window](#)

Wiley InterScience Logo

### Laser Light Scattering: Some Recent Developments

[Print](#) | [Close Window](#)

**Figure 10.** (a) Schematic view of a novel differential refractometer (commercialized by Jianke Instrument Co. Ltd, Anhui, People's Republic of China), which consists of a pinhole, a differential refractometer cuvette, a lens ( $f = 20$  cm), and a PSD. All components are rigidly mounted on a long metal board (~100 cm). (b) Light path in which one compartment of the cuvette contains a solvent with refractive index  $n$ , and the other contains a solution with slightly different refractive index  $n = n_0 + \Delta n$ . The cuvette and angles  $\theta_1$ ,  $\theta_2$  and  $\theta_3$  (actually very small,  $\sim 0.01$  radian) are enlarged to make the light path distinct.



Encyclopedia of Polymer Science and Technology  
Published by John Wiley & Sons, Inc.

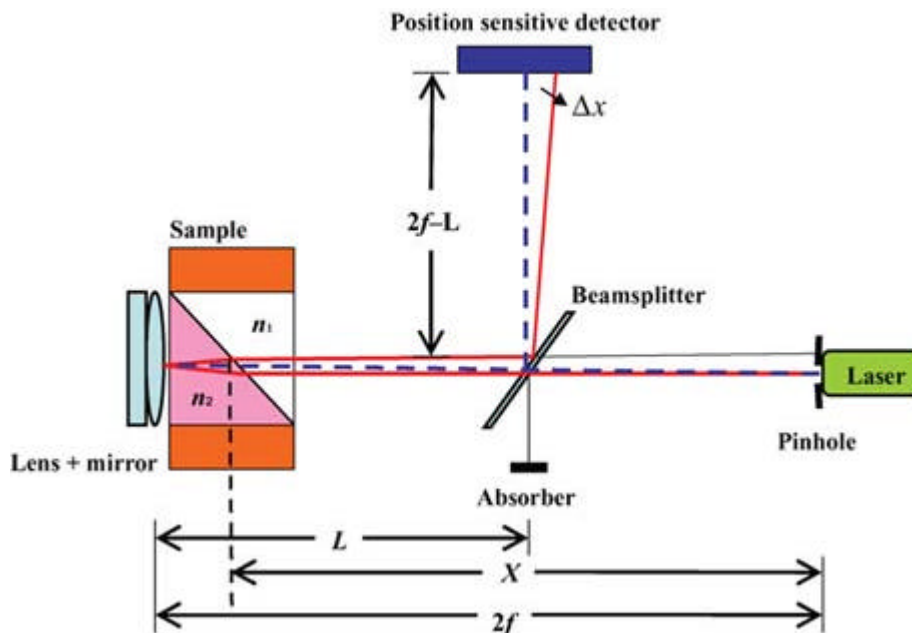
[Print](#) | [Close Window](#)

Wiley InterScience Logo

## Laser Light Scattering: Some Recent Developments

[Print](#) | [Close Window](#)

**Figure 11.** Schematic view of a novel portable differential refractometer, which was a further modified version of Figure 10 by placing a combination of a convex lens (focal length =  $2f = 350$  mm) and a laser mirror just after the divided cells and addition of a beam splitter ( $L = 180 \pm 1$  mm)



Encyclopedia of Polymer Science and Technology  
Published by John Wiley & Sons, Inc.

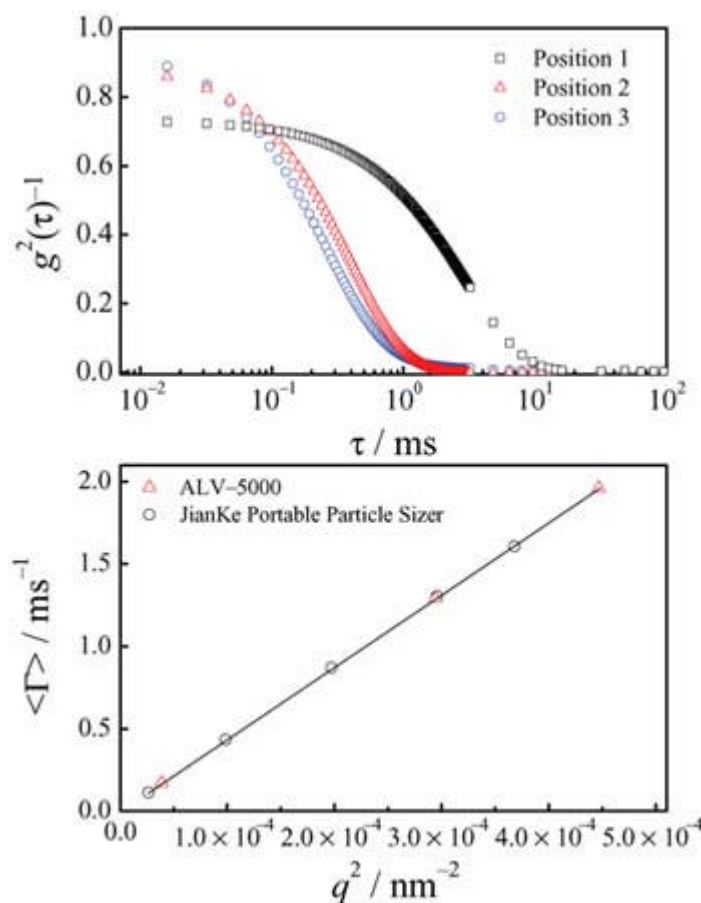
[Print](#) | [Close Window](#)

 Wiley InterScience Logo

## Laser Light Scattering: Some Recent Developments

[Print](#) | [Close Window](#)

**Figure 12.** Top: The normalized intensity-intensity time correlation function  $g^2(\tau) - 1$  via  $\tau$  from 16  $\mu\text{s}$  to 589 ms measured by portable particle sizer; Bottom: Dependence of  $\Gamma$  and  $q^2$  for polystyrene nanoparticles dispersed in D.I. water at 25.0°C.



Encyclopedia of Polymer Science and Technology  
Published by John Wiley & Sons, Inc.

[Print](#) | [Close Window](#)